




A Defect in Influenza A Virus Particle Assembly Specific to Primary Human Macrophages

Sukhmani Bedi,^a Takeshi Noda,^b Yoshihiro Kawaoka,^{c,d}  Akira Ono^a

^aDepartment of Microbiology and Immunology, University of Michigan Medical School, Ann Arbor, Michigan, USA

^bLaboratory of Ultrastructural Virology, Department of Virus Research, Institute for Frontier Life and Medical Sciences, Kyoto University, Kyoto, Japan

^cDivision of Virology, Department of Microbiology and Immunology, Institute of Medical Science, University of Tokyo, Tokyo, Japan

^dDepartment of Pathobiological Sciences, University of Wisconsin—Madison, Madison, Wisconsin, USA

ABSTRACT Influenza A virus (IAV) propagates efficiently in epithelial cells, its primary target in the respiratory tract. In contrast, productive infection of most IAV strains is either blocked or highly inefficient in macrophages. The exact nature of the defect in IAV replication in human macrophages remains unknown. In this study, we showed that even compared to a monocytic cell line differentiated to macrophage-like cells, primary human monocyte-derived macrophages (MDM) are inefficient in IAV production, despite comparable levels of expression of viral glycoproteins at the plasma membrane. Correlative fluorescence scanning electron microscopy revealed that formation of budding structures at the cell surface is inefficient in MDM even though clustering of a viral glycoprotein, hemagglutinin (HA), is observed, suggesting that a step in IAV particle assembly is blocked in MDM. Using an *in situ* proximity ligation assay, we further determined that HA associates with neuraminidase (NA) but fails to associate with another viral transmembrane protein, M2, at the MDM plasma membrane. Notably, the defects in HA-M2 association and particle assembly in MDM were reversed upon cytochalasin D treatment that inhibits actin polymerization. These results suggest that HA-M2 association on the plasma membrane is a discrete step in IAV production, which is susceptible to suppression by actin cytoskeleton in MDM. Virus release remained inefficient in MDM upon cytochalasin D treatment, suggesting the presence of an additional defect(s) in virus release in this cell type. Overall, our study revealed the presence of multiple cell-type-specific mechanisms negatively regulating IAV production at the plasma membrane in MDM.

IMPORTANCE Identification of host cell determinants promoting or suppressing replication of viruses has been aided by analyses of host cells that impose inherent blocks on viral replication. In this study, we show that primary human MDM, which are not permissive to IAV replication, fail to support virus particle formation. This defect is specific to primary human macrophages, since a human monocytic cell line differentiated to macrophage-like cells supports IAV particle formation. We further identified association between two viral transmembrane proteins, HA and M2, on the cell surface as a discrete assembly step, which is defective in MDM. Defective HA-M2 association and particle budding, but not virus release, in MDM are rescued by disruption of actin cytoskeleton, revealing a previously unknown, negative role for actin, which specifically targets an early step in the multistep IAV production. Overall, our study uncovered a host-mediated restriction of association between viral transmembrane components during IAV assembly.

KEYWORDS actin, influenza, macrophages, plasma membrane, virus assembly

Received 30 August 2018 Accepted 17 September 2018 Published 23 October 2018

Citation Bedi S, Noda T, Kawaoka Y, Ono A. 2018. A defect in influenza A virus particle assembly specific to primary human macrophages. *mBio* 9:e01916-18. <https://doi.org/10.1128/mBio.01916-18>.

Editor Kanta Subbarao, NIAID, NIH

Copyright © 2018 Bedi et al. This is an open-access article distributed under the terms of the [Creative Commons Attribution 4.0 International license](https://creativecommons.org/licenses/by/4.0/).

Address correspondence to Akira Ono, akiraono@umich.edu.

Influenza A virus (IAV) is a negative-strand RNA virus that mainly infects and replicates in epithelial cells in the respiratory tract. However, the virus has also been shown to infect other cell types such as macrophages, dendritic cells, and mast cells *ex vivo* (1–3). Host-cell-specific differences have been observed for various properties of IAV, including morphology and replication (for example, see references 4 to 8). These differences could be due to differences in expression levels or functions of host cellular proteins between cell types. In cases where cell-type-specific differences affect productive infection of a virus, detailed comparison between permissive and nonpermissive cell types often leads to identification of virus cofactors (7, 9–12) or host factors that restrict replication of viruses (8, 13–16). This approach, which often determines the specific function of the host factor of interest even prior to the identity of the factor, can serve as a complementary approach to genome-wide approaches (17–26).

Ex vivo infection studies have shown that in comparison to epithelial cells, macrophages are less permissive or nonpermissive to productive infection of seasonal IAV strains (27–33). Murine macrophages are nonpermissive to IAV replication (27, 29, 33, 34). Primary human blood-derived or alveolar macrophages do support seasonal IAV replication at detectable levels, although they are still much less permissive to virus growth than human epithelial cells (28, 30, 31, 34). As for the defective stages of the IAV life cycle, a block at the entry stage of infection has been identified in murine macrophages for most H1N1 strains (27, 29, 33). In addition, the presence of a defect(s) at a later stage has been known for IAV infection in murine macrophages (29, 33). However, there are apparently conflicting data as to whether the defect is at pre- or posttranslation stage (29, 33). Moreover, the mechanism in either case has yet to be determined. In contrast to murine macrophages, human macrophages support early stages of replication of all tested IAV strains yet are unable to complete the virus life cycle (33). While the defect appears to be posttranslational, the exact nature of this defect in human macrophages and the molecular mechanism behind it are not known.

Determining the nature of the human macrophage-specific defect in IAV replication is likely to advance our understanding of the roles played by cellular functions in late phases of the IAV life cycle and potentially facilitate identification of human host factors involved in this process. In the current study, we used primary human monocyte-derived macrophages (MDM) in order to identify the defective step in IAV replication in human macrophages. We show that MDM support early stages of the IAV assembly process, i.e., trafficking of the viral glycoproteins hemagglutinin (HA), neuraminidase (NA), and the ion channel protein M2 to the plasma membrane, but are inefficient at virus particle formation and subsequent virus release. This defect in virus particle formation and release is specific to primary MDM, since a monocytic cell line, THP1, when differentiated into macrophage-like cells, supports efficient virus particle production. Notably, we observed that the association of HA with M2 on the plasma membrane, as determined by the close proximity of <40 nm, is highly inefficient in MDM relative to the differentiated THP1 cells. In contrast, HA and NA associate efficiently on the surface of MDM. The defective association between HA and M2 is rescued in MDM upon treatment with an actin polymerization inhibitor, cytochalasin D, whereas this defect is recreated in differentiated THP1 cells by treatment with jasplakinolide (Jasp), which promotes actin polymerization. Consistent with the restoration of HA-M2 association in MDM, treatment with cytochalasin D also increases formation of budding structures in this cell type. However, virus release is not restored in MDM upon cytochalasin D treatment, suggesting the presence of an additional block in IAV assembly/release in this cell type. Overall, this study has identified virus particle formation, more specifically association between HA and M2, as a step defective in the IAV life cycle in primary human macrophages and revealed that this macrophage-specific block of IAV assembly requires actin polymerization.

RESULTS

MDM are inefficient in supporting productive IAV infection relative to differentiated THP1 cells. To determine the extent to which human epithelial cells and

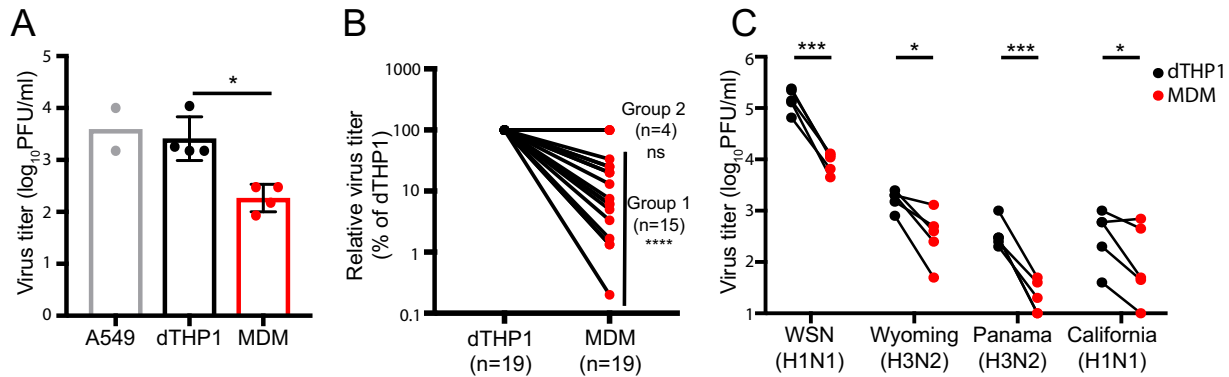


FIG 1 MDM are defective in productive IAV infection. (A) A549 cells, dTHP1 cells, and MDM were infected with WSN at MOI 0.01. Infectious virus titers in culture supernatants were measured at 11 hpi. (B) Infectious virus titers in culture supernatants were measured for WSN-infected dTHP1 cells and MDM at 24 hpi. For all tested donors, the relative virus titers in MDM cultures were calculated in comparison to the titer in dTHP1 cell cultures tested in parallel within the same experiment. Two groups of donors (groups 1 and 2) were designated based on the reduction in the titers or lack thereof. For group 1, the values for virus titers were in the range of 1.9 to 5.07 log₁₀ PFU/ml. For group 2, the values were identical to those of corresponding dTHP1 cultures and in the range of 4.39 to 5.17 log₁₀ PFU/ml. (C) dTHP1 and MDM (group 1) were infected with the given IAV strains at MOI 0.01, and infectious virus titers in culture supernatants at 24 hpi were determined by plaque assays using MDCK cells that have been passaged 20 to 30 times. Each circle represents an independently prepared culture. A black and a red circle connected by a line represent each independent experiment. For panel A, data are shown as mean \pm SD. *, $P < 0.05$; ***, $P < 0.001$; ****, $P < 0.0001$; ns, nonsignificant.

macrophages differ in their ability to support productive IAV infection, we compared infectious IAV release from three different human cell types: the lung-derived epithelial cell line A549; the monocytic cell line THP1, which has been differentiated to adopt macrophage-like morphology (dTHP1); and primary monocyte-derived macrophages (MDM). The dTHP1 cells were obtained via treatment of THP1 cells with phorbol 12-myristate 13-acetate (PMA) and vitamin D3 for 2 to 3 days. A549, dTHP1, and MDM were infected with the laboratory strain A/WSN/1933 (H1N1) (WSN) at a multiplicity of infection (MOI) of 0.01 based on the PFU of virus stocks determined using MDCK cells. At 11 h postinfection (hpi), we observed that virus titers in MDM culture supernatants were up to 100-fold reduced in comparison to that in A549 culture supernatants. Unexpectedly, virus titers in culture supernatants were similar between A549 and dTHP1 cells (Fig. 1A). Since dTHP1 cells support influenza virus replication efficiently unlike MDM and yet belong to the same cellular lineage, to facilitate the analyses of the MDM-specific defect(s), we chose to compare IAV replication in MDM with that in dTHP1 cells in subsequent experiments. We noticed that while MDM isolated from the vast majority of the tested human donors showed a defect in productive IAV infection relative to dTHP1 at 24 hpi (denoted as group 1 in Fig. 1B), MDM from some donors (denoted as group 2 in Fig. 1B; ~20%) showed no significant difference. Therefore, to identify the MDM-specific defect, the subsequent experiments were performed using MDM from the donors in group 1. In particular, in the mechanistic experiments (see Fig. 3 to 7), we verified in each experiment that MDM used show 10- to 20-fold reduction in the supernatant virus titers or released vRNA relative to dTHP1 cells at the indicated time point of the corresponding assays (data not shown).

To assess whether other IAV strains also replicate inefficiently in MDM relative to dTHP1 cells, we compared productive infection in dTHP1 cells and MDM of three previously or currently circulating IAV strains, in addition to WSN: A/Wyoming/03/2003 (H3N2) [Wyoming (H3N2)], A/Panama/2007/1999 (H3N2) [Panama (H3N2)], and A/California/04/2009 (H1N1) [California (H1N1)]. Infectious virus titers of all tested IAV strains, as measured by the plaque assay, were reduced by 10- to 50-fold in MDM in comparison to dTHP1 cells (Fig. 1C). These data suggest that MDM are highly inefficient at producing infectious IAV particles in comparison to dTHP1 cells.

Both efficiency of virus release and infectivity of released particles are impaired in infected MDM relative to infected dTHP1 cells. The results shown above and the results of time course experiments suggest that infectious virus release is reduced in MDM relative to dTHP1 cells even though flow cytometry using anti-vRNP

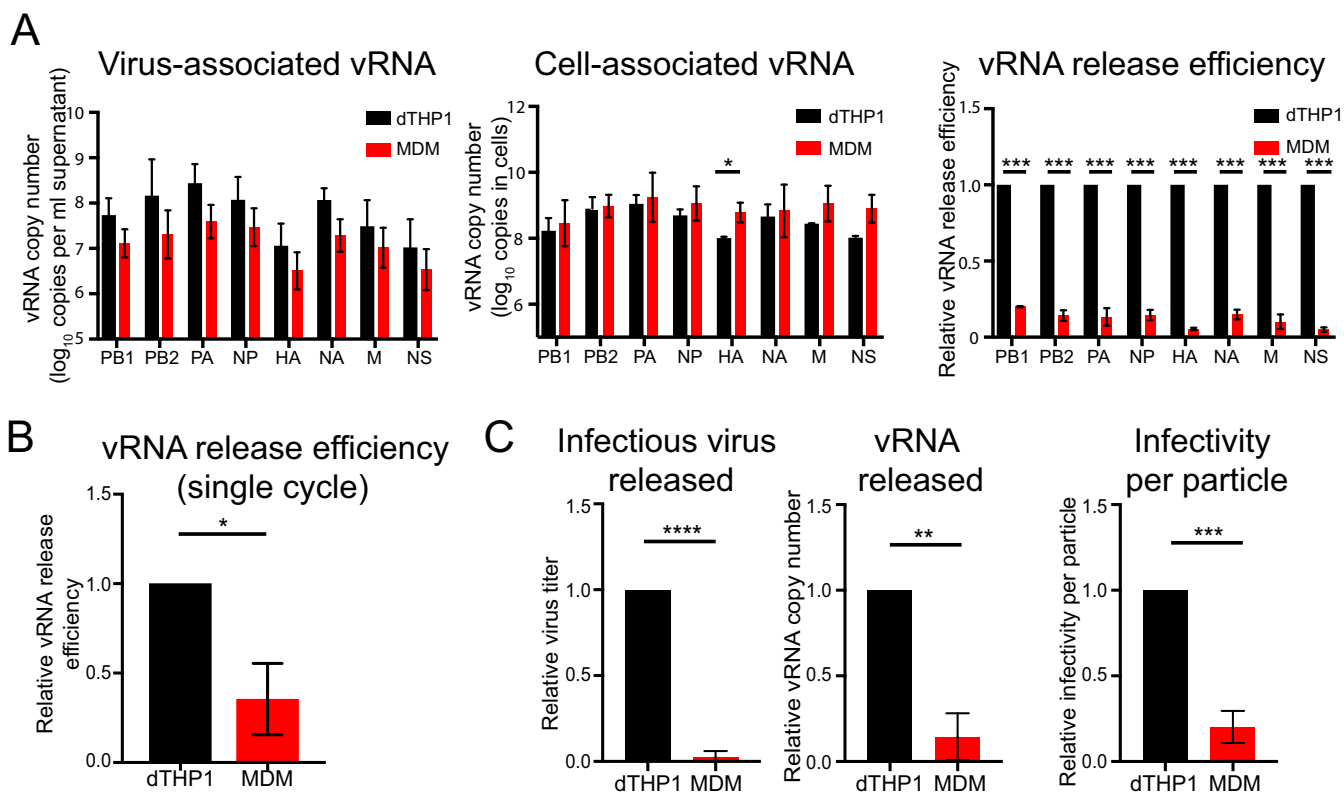


FIG 2 Both efficiency of virus release and infectivity of released particles are lower in MDM than in dTHP1 cells. dTHP1 cells and MDM were infected with WSN at MOI 0.1. (A) vRNA copy numbers were measured in lysates of virus pelleted from cell culture supernatants and cell lysates at 20 hpi. vRNA release efficiency was calculated as the ratio of number of vRNA copies in virus lysates to total number of vRNA copies (cell + virus) for each vRNA segment. Note that in most cases (except for cell-associated HA vRNA) differences between dTHP1 cells and MDM were not significant for virus-associated and cell-associated vRNA levels, which were compared as pooled data. However, vRNA release efficiency calculated for individual experiments showed a significant reduction in MDM cultures relative to dTHP1 cell cultures. (B) vRNA release efficiency was measured for infected dTHP1 cells and MDM at 12 hpi. To prevent the second cycle of infection, 10 μ g/ml C179 was added to the cultures at 2 hpi. (C) PB2 vRNA copy number and virus titer were measured in dTHP1 and MDM culture supernatants at 16 hpi. Infectivity per particle was calculated as the ratio of virus titer to PB2 vRNA copy number in culture supernatants. Data are from experiments done with MDM from at least three independent donors and shown as mean \pm SD. *, $P < 0.05$; **, $P < 0.01$; ***, $P < 0.001$, ****, $P < 0.0001$.

antibody (clone 61A5 [35]) showed that similar fractions of cells in the cultures are infected (Fig. 1; see also Fig. S1 in the supplemental material). We sought to address whether the reduction in viral titers in MDM culture supernatants is due to a reduction in infectivity of released particles or whether it is due to a reduction in release of physical particles. To this end, we used viral RNA (vRNA) release as a surrogate to measure release of physical particles from dTHP1 cells and MDM. Numbers of vRNA copies released from MDM were 7- to 8-fold reduced in comparison to that from dTHP1 cells for all eight vRNA segments. However, there were no significant decreases in cell-associated vRNA levels in MDM relative to dTHP1 cells, indicating that MDM support viral RNA replication and earlier steps as efficiently as dTHP1 cells. vRNA release efficiency was calculated as the ratio of number of vRNA copies in virus pellets from cell culture supernatants to the total number of vRNA copies (cell + virus). For all eight vRNA segments, we observed a 5- to 10-fold reduction in vRNA release efficiency in MDM relative to dTHP1 cells (Fig. 2A). We also measured vRNA release efficiency in dTHP1 cells and MDM after a single round of virus replication (Fig. 2B). To block virus entry after the first round on infection, cells were treated with medium containing 10 μ g/ml C179, a neutralizing antibody that binds to the HA stem (36, 37), at 2 hpi. At 12 hpi, we observed a 2- to 3-fold reduction in vRNA release efficiency in MDM relative to dTHP1 cells. These data suggest that efficiency of physical viral particle release from MDM is reduced in comparison to that from dTHP1 cells in the context of both single and multiple rounds of virus replication.

Importantly, the reduction in vRNA release (7- to 8-fold) from MDM does not entirely account for reduction in infectious virus release (up to 50-fold) (Fig. 2C). The ratio of released PFU (representing infectious virions) to released vRNA (representing total number of particles) was calculated as the infectivity per particle. Infectivity per particle for virus particles released from MDM was 5- to 6-fold reduced versus that released from dTHP1 cells (Fig. 2C). Overall, our data suggest that the total number of virus particles released as well as the infectivity of released virus particles is reduced in MDM relative to dTHP1 cells.

Formation of budding structures is inefficient in MDM relative to dTHP1 cells despite similar levels of viral glycoprotein expression at the plasma membrane.

We observed using flow cytometry that total expression levels of vRNP, HA, and M1 are comparable between dTHP1 cells and MDM in both the size of positive cell populations and the expression levels per cell (Fig. S1 and S2), indicating that protein translation and earlier steps are unlikely to be impaired in MDM. Henceforth, we focused on steps after viral protein translation: virus assembly, budding, and release. Virus assembly is initiated by targeting of the glycoproteins HA and NA to the plasma membrane (38–40). The third transmembrane protein M2 is also recruited to the assembly sites at the plasma membrane and allows for completion of the virus budding process (39, 41). To determine whether trafficking of the three glycoproteins occurs similarly in dTHP1 cells and MDM, we next compared levels of HA, NA, and M2 proteins on the surface of WSN-infected cells. We found that sizes of cell populations positive for surface expression of the three proteins are comparable between MDM and dTHP1 cells (Fig. 3A and B). The mean fluorescence intensity (MFI) for the three viral proteins in positive cell populations was also similar between MDM and dTHP1 cells (Fig. 3C), indicating that trafficking of viral glycoproteins to the plasma membrane is comparable between MDM and dTHP1 cells.

We next asked whether dTHP1 cells and MDM expressing HA on the cell surface support virus particle formation. To address this question in a single cell basis, we performed correlative fluorescence and scanning electron microscopy (CFSEM) in which we first identify cells with surface HA expression using fluorescence microscopy and then examine formation of virus particle-like buds on the surface of the same cells using scanning electron microscopy (SEM). Fluorescence microscopy showed that HA is uniformly distributed on the surface of both dTHP1 cells and MDM with some local accumulation. These HA-enriched clusters or puncta, which likely represent sites of virus assembly, were clearly distinguished on the surface of infected cells after the median filter was applied to the confocal images to remove signal for uniformly distributed nonpunctate HA. These HA-enriched sites often corresponded to budding structures with a diameter of approximately 100 nm on the surface of WSN-infected dTHP1 cells (Fig. 4A). Very few budding structures with the similar size were observed on the surface of mock-infected cells. MDM also form ~100-nm virus particle-like buds on the surface in HA-positive cells, albeit the number of buds observed in MDM was markedly lower than in dTHP1 cells (Fig. 4A). To assess the formation of budding structures quantitatively, we counted the number of HA-positive puncta and the number of virus particle-like buds within the same-sized area (100 μm^2 in size) of each cell. Even though MDM showed higher numbers of HA-positive puncta on the cell surface than dTHP1 cells, the numbers of virus buds were drastically reduced in MDM relative to dTHP1 cells (Fig. 4B). Overall, these results indicate that virus particle assembly and budding are inefficient in MDM despite efficient trafficking of HA, NA, and M2 to the plasma membrane.

Association between HA and M2 is impaired in MDM but not in dTHP1 cells.

Based on results shown above, we hypothesize that local coenrichment of HA, NA, and M2, which leads to formation of virus assembly sites, is not efficient in MDM relative to dTHP1 cells. To compare formation of the putative assembly sites between dTHP1 cells and MDM, we used *in situ* proximity ligation assay (PLA). PLA allows for detection of two proteins localized within 40-nm distance of each other and has been used to visualize IAV assembly sites on the plasma membrane (42). In addition to measuring PLA signal

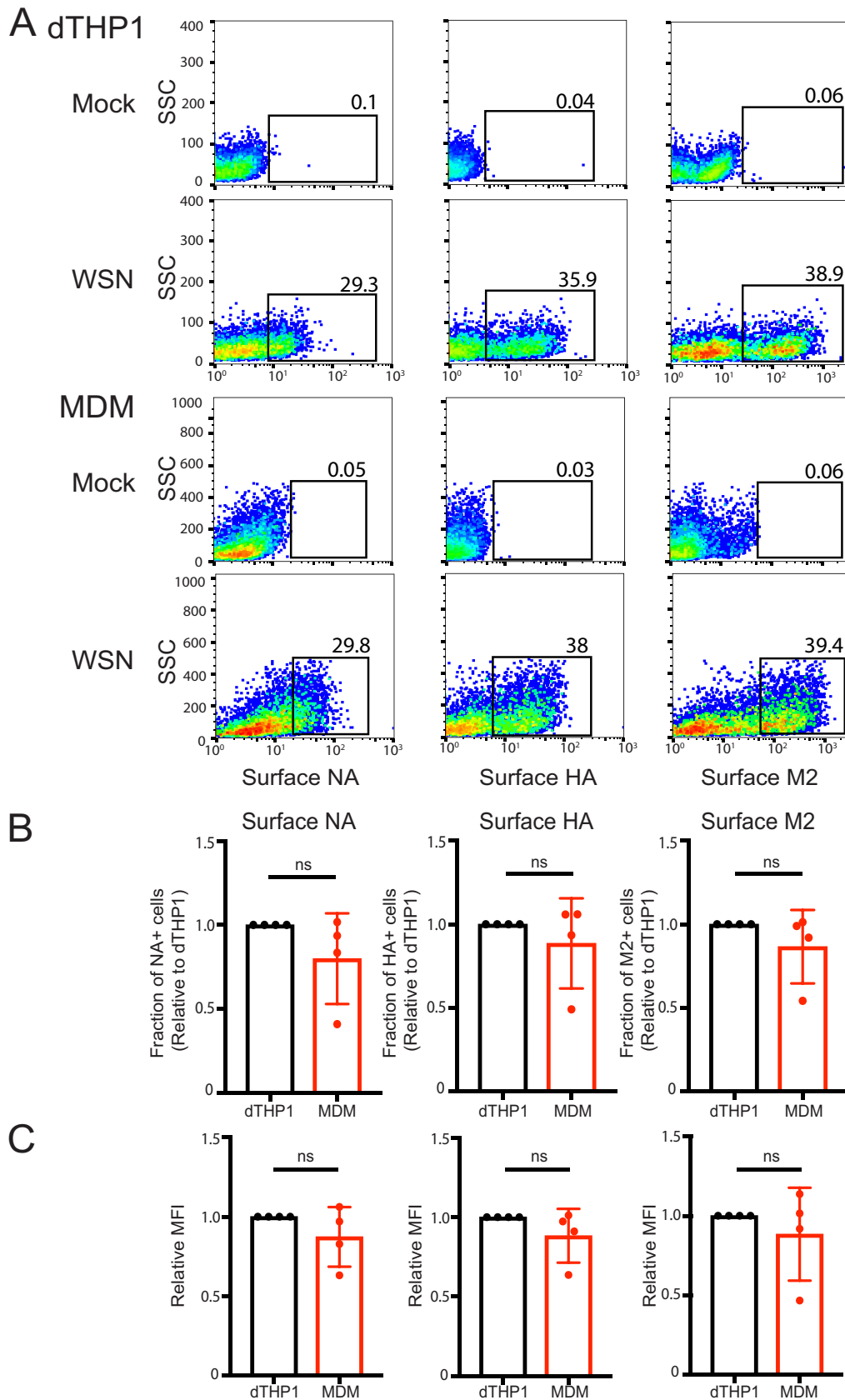


FIG 3 MDM are efficient at trafficking of viral glycoproteins to the cell surface. dTHP1 cells and MDM were infected with WSN at MOI 0.1. (A) Infected cells were analyzed for cell surface expression of HA, NA, and M2 by flow cytometry at 16 (Continued on next page)

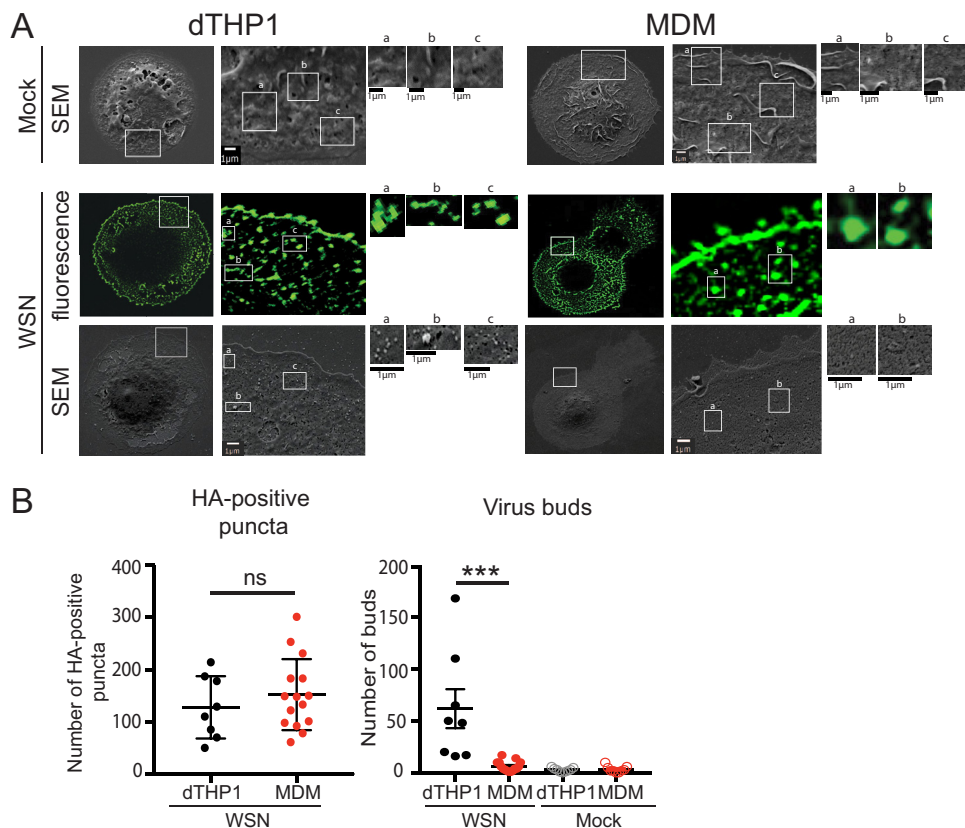


FIG 4 MDM are defective in virus bud formation despite expression of HA on the cell surface. dTHP1 cells and MDM grown on gridded coverslips were infected with WSN at MOI 0.1 for 20 h. Cells were fixed and immunostained with anti-HA. After identification of HA-positive cells by confocal fluorescence microscopy, cells were prepared for SEM. The same cells were identified based on grid positions and analyzed by SEM. (A) Representative SEM images for mock-infected and WSN-infected HA-positive cells are shown in the top and bottom rows, respectively. Fluorescence images corresponding to the SEM images of WSN-infected cells are shown in the middle row. Boxed areas are magnified and shown on the right of original images. Alphabetic labels are used to distinguish between individual boxed areas. (B) The numbers of HA-positive puncta identified in fluorescence images (left panel) and ~100-nm buds identified in SEM images (right panel) were counted within the same-size area (100 μm^2 in size) in each cell. Data are shown for 8 to 15 cells from two independent experiments. Error bars represent standard error of mean. ***, $P < 0.0001$; ns, nonsignificant.

between the given pair of proteins, we also costained cells for cell surface NA to identify infected cells. As a negative control, we performed PLA between HA and transferrin receptor (TfR). TfR does not associate with lipid rafts (43), the plasma membrane microdomains associated with IAV assembly sites (39, 44). Infected dTHP1 cells showed high PLA signal for HA-M2 association. In contrast, infected MDM showed very few PLA spots between HA and M2 (Fig. 5A and C). As expected, no PLA signal was observed between HA and M2 in mock-infected cells or between HA and TfR in infected cells (Fig. 5A). The majority (80% to 90%) of surface NA-positive MDM and dTHP1 cells express HA and M2 on their surface at comparable levels (Fig. S3). Therefore, the significant reduction in HA-M2 PLA signal in MDM relative to dTHP1 cells is not due to the lack of expression of HA and/or M2 in NA-positive cells.

FIG 3 Legend (Continued)

hpi. Representative flow plots for mock-infected (top row) and virus-infected (bottom row) cells are shown. Percentages of cells positive for viral proteins (boxed) are shown. Due to differences in the side scatter (SSC) profile between dTHP1 cells and MDM, the y axis (SSC) range is different between the two cell types. (B) Percentages of cells positive for surface expression of NA, HA, and M2 are compared between dTHP1 and MDM. (C) Relative MFIs for surface signal of indicated proteins for positive cell populations (gated in panel A) are shown. Data are shown as mean \pm SD and are from at least three independent experiments. ns, nonsignificant.

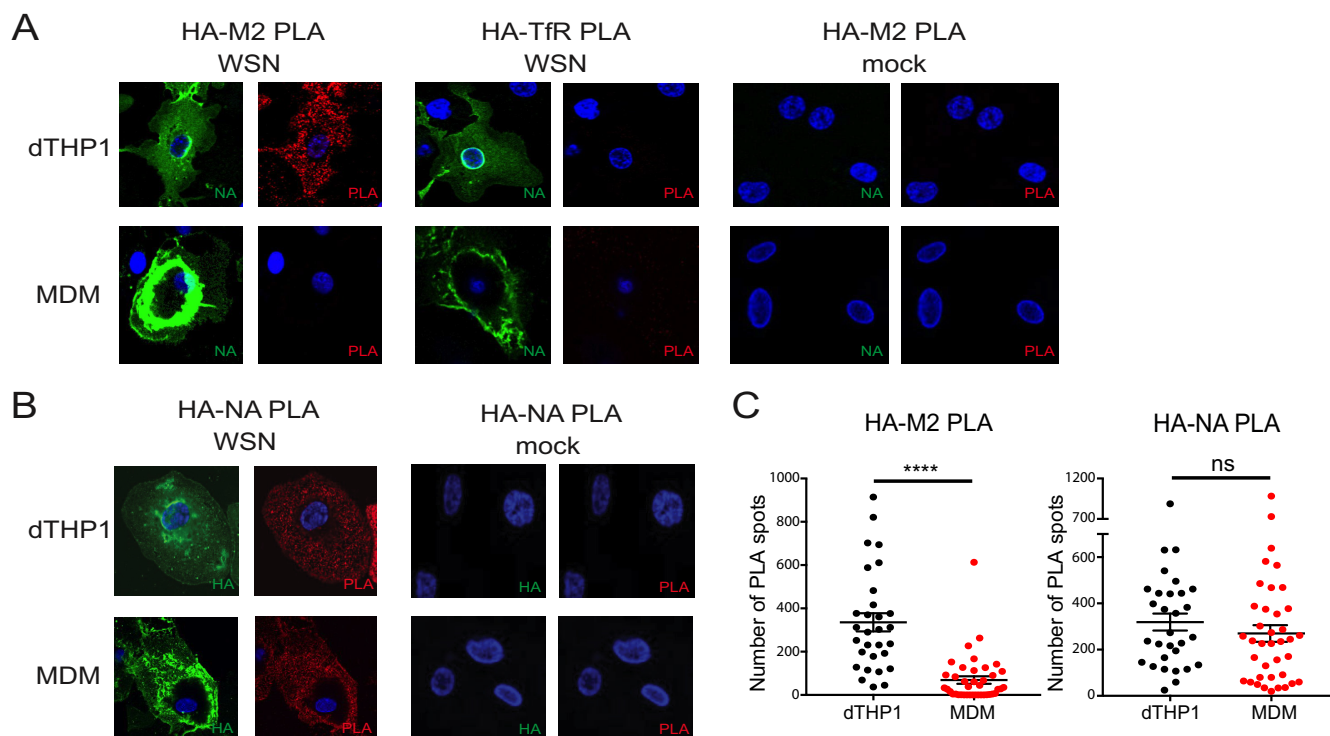


FIG 5 Association between HA and M2 is defective in MDM relative to dTHP1 cells. dTHP1 cells and MDM were infected with WSN at MOI 0.1 for 16 h. (A) Cells were examined by PLA using goat anti-HA and mouse anti-M2 or goat anti-HA and mouse anti-TfR antibodies. To identify infected cells, surface NA was also detected by rabbit anti-NA. Nuclei were stained with DAPI (blue). Representative maximum intensity projection images, which were reconstructed from Z-stacks corresponding to the focal planes ranging from the middle plane of the nucleus to the bottom of the cells, are shown. (B) Cells were examined by PLA using mouse anti-HA and rabbit anti-NA antibodies. Goat anti-HA was used for detection of infected cells. Representative maximum intensity projection images are shown as in panel A. Note regions of intense NA (in panel A) and HA (in panel B) signal on the surface of MDM due to the presence of membrane ruffles. (C) Number of PLA spots was counted for each cell. Data are shown for three independent experiments, and 8 to 10 cells were analyzed per experiment. These experiments were performed in parallel with the experiments shown in Fig. 3 using MDM from the same donors. Error bars represent standard error of mean. ****, $P < 0.0001$; ns, nonsignificant.

To determine whether the defect in association between transmembrane proteins in MDM is specific to HA and M2 or whether association between other pairs of viral transmembrane proteins is defective as well, we next measured PLA signal between HA and NA. In this case, to identify infected cells, we costained cells for cell surface HA using an antibody different from the one used for PLA. PLA signal between HA and NA was similar for dTHP1 cells and MDM, suggesting that HA and NA associate with each other as efficiently on the surface of MDM as on dTHP1 cells (Fig. 5B and C). Overall, our data indicate that association between HA and M2 is a virus assembly step specifically impaired in MDM.

Inhibition of actin polymerization increases HA-M2 PLA and bud formation in MDM. HA associates with lipid rafts on the plasma membrane, while M2 mainly localizes in non-lipid raft areas (39, 44). It is suggested that M2 is recruited to cholesterol-rich lipid rafts during IAV particle assembly (45, 46); however, host cell functions and factors that regulate this step are not known. It is possible that in MDM, HA-containing plasma membrane microdomains stay segregated from those containing M2, leading to defective association between the two glycoproteins. The cortical actin cytoskeleton, a network of filaments that underlies and interacts with the plasma membrane, is suggested to play a role in formation and maintenance of plasma membrane microdomains (47–49). Therefore, we next asked whether the actin network regulates the association between HA and M2 in dTHP1 cells and MDM. Infected cells were treated with cytochalasin D (Cyto D), an inhibitor of actin polymerization, at 14 hpi for 2 h, fixed, and examined for HA-M2 association using PLA. Phalloidin staining confirmed that Cyto D disrupts the cellular actin network in both dTHP1 cells and MDM

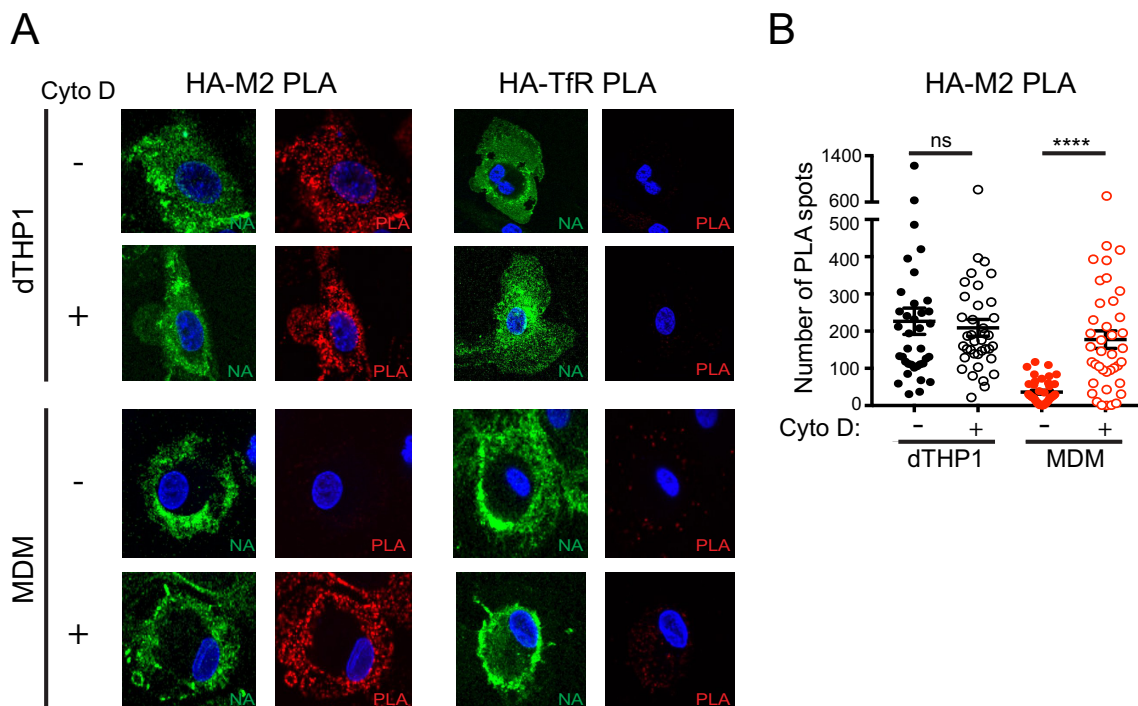


FIG 6 Cytochalasin D treatment restores HA-M2 PLA in MDM to levels comparable to that in dTHP1 cells. dTHP1 cells and MDM were infected with WSN at MOI 0.1. At 14 hpi, cells were treated with vehicle control (DMSO) or 20 μ M cytochalasin D (Cyto D) for 2 h before fixation. (A) Cells were analyzed as in Fig. 5A. Representative maximum intensity projection images are shown. (B) Number of PLA spots was counted for each cell. These experiments were performed in parallel with the experiments shown in Fig. S4 using MDM from the same donors. Data are from at least three independent experiments, and 8 to 10 cells were analyzed per experiment. Error bars represent standard error of mean. ****, $P < 0.0001$; ns, nonsignificant.

under these treatment conditions (Fig. S4A). Infected dTHP1 cells showed high PLA signal for HA-M2 association under both vehicle- and Cyto D-treated conditions. As observed in Fig. 5A, vehicle-treated MDM showed very few PLA spots between HA and M2. In contrast, Cyto D-treated MDM showed PLA signal between HA and M2 at levels similar to that observed for dTHP1 cells (Fig. 6A and B). No PLA signal was observed between HA and TfR in untreated or Cyto D-treated dTHP1 cells and MDM. The increase in HA-M2 PLA signal upon Cyto D treatment of MDM was not due to an increase in surface expression of HA and M2 in drug-treated cells, as shown by the flow cytometry analysis (Fig. S4B and C). These results suggest that actin polymerization suppresses HA-M2 association in MDM.

We next asked whether treatment with Cyto D restores virus budding in MDM. To this end, we performed CFSEM of dTHP1 cells and MDM treated with either vehicle or Cyto D at 14 hpi for 4 h and examined virus bud formation in cells expressing HA on the cell surface. We counted the number of virus particle-like buds (~ 100 nm in diameter) within the same-sized area ($100 \mu\text{m}^2$ in size) of each cell. Consistent with the results shown in Fig. 4, vehicle-treated, HA-positive MDM showed significantly lower numbers of buds on the cell surface than vehicle-treated, HA-positive dTHP1 cells. Notably, Cyto D treatment significantly increased the number of buds on the surface of MDM to levels comparable to those in vehicle-treated dTHP1 cells (Fig. 7A and B). Cyto D-treated dTHP1 cells showed no significant increase in bud formation relative to vehicle-treated dTHP1 cells. Very few such budding structures corresponding to the size of IAV particles were observed on the surface of untreated or Cyto D-treated, mock-infected dTHP1 cells and MDM (Fig. 7B). These data suggest that disruption of the actin cytoskeleton promotes IAV particle assembly in MDM. To determine whether the increase in efficiency of bud formation leads to an increase in virus release, we measured the PB2 vRNA release efficiency as shown in Fig. 2A. Again, vRNA release efficiency was 4- to 5-fold reduced in vehicle-treated MDM cultures relative to vehicle-

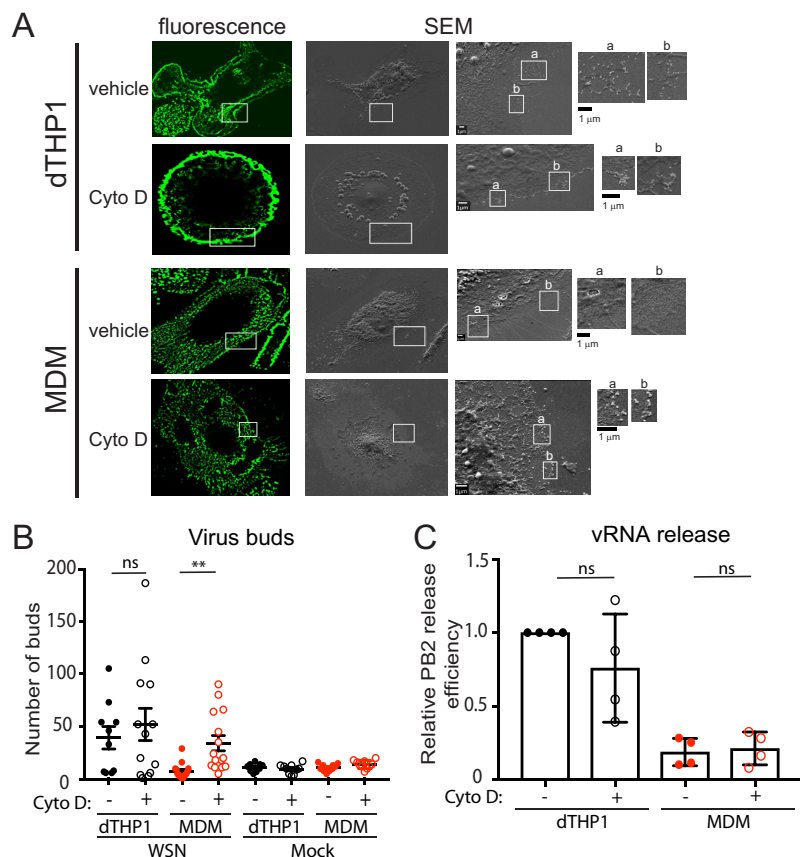


FIG 7 Cytochalasin D treatment increases bud formation in MDM to levels comparable to that in dTHP1 cells. dTHP1 cells and MDM were infected with WSN at MOI 0.1. At 14 hpi, cells were treated with vehicle control (DMSO) or 20 μ M Cyto D for 4 h before fixation and immunostaining with anti-HA. After identification of HA-positive cells by confocal fluorescence microscopy, cells were processed for SEM. The same cells were identified based on grid positions and analyzed by SEM. (A) Representative SEM images for WSN-infected HA-positive cells are shown. Fluorescence images corresponding to the SEM images are also included. Boxed areas for SEM images are magnified and shown on the right of original images. Alphabetic labels are used to distinguish between the individual boxed areas. (B) The number of \sim 100-nm buds identified in SEM images was counted within the same-size area ($100 \mu\text{m}^2$ in size) in each cell. Data are shown for 10 to 20 cells from three independent experiments. (C) vRNA release efficiency was measured in infected MDM and dTHP1 cell cultures treated with DMSO or Cyto D for 4 h. For panel B, error bars represent standard error of mean. For panel C, error bars represent SD. **, $P < 0.01$; ns, nonsignificant.

treated dTHP1 cell cultures. Contrary to expectation, Cyto D treatment did not enhance vRNA release efficiency (Fig. 7C). We also did not observe any increase in infectious virus titers (Fig. S4D) in supernatants of MDM cultures upon Cyto D treatment. These results indicate that disruption of the actin cytoskeleton promotes virus budding but not virus release. It is conceivable that there is an additional MDM-specific block in the late assembly/release stages of the IAV life cycle, which cannot be reversed by Cyto D. Overall, these data show that virus particle assembly, more specifically HA-M2 association, is negatively regulated by the actin cytoskeleton in MDM.

Promotion of actin polymerization reduces HA-M2 PLA in dTHP1 cells. Since inhibition of actin polymerization restores association of HA and M2 in MDM, we next asked whether promoting actin polymerization inhibits HA-M2 association in dTHP1 cells. To this end, infected dTHP1 cells were treated with jasplakinolide (Jasp), which nucleates and stabilizes actin polymerization, at 14 hpi for 2 h and examined for HA-M2 association using PLA at 16 hpi as in Fig. 6. Two hours of Jasp treatment reduced HA-M2 PLA in 50% of the examined dTHP1 cells, while the remaining infected cell population showed HA-M2 PLA signal comparable to that in untreated cells (data not shown). We

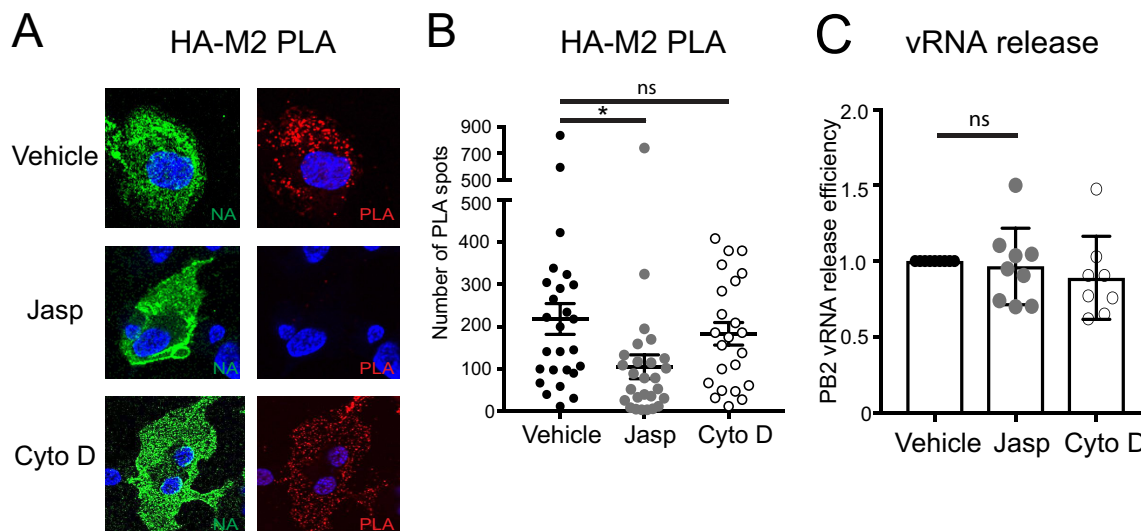


FIG 8 Jasplakinolide treatment reduces HA-M2 PLA in dTHP1 cells. dTHP1 cells were infected with WSN at MOI 0.1. (A and B) At 10 hpi, cells were treated with vehicle control (0.5% ethanol), 1 μ M jasplakinolide (Jasp), or 20 μ M Cyto D for 4 h before fixation. (A) Representative maximum intensity projection images are shown as in Fig. 5A. (B) Number of PLA spots was counted for each cell, and data are shown for 7 to 10 cells per experiment. (C) vRNA release efficiency was measured in infected dTHP1 cell cultures treated with vehicle, Jasp, and Cyto D for 4 h. Data are from at least three independent experiments. For panel B, error bars represent standard error of mean. For panel C, error bars represent SD. *, $P < 0.05$; ns, nonsignificant.

reasoned that high HA-M2 PLA signal in 50% of Jasp-treated dTHP1 cells is due to preexisting association between HA and M2 at the time of Jasp addition. Therefore, we next examined the effect of Jasp on HA-M2 association at an earlier time point in infection when preexisting HA-M2 coclusters are unlikely to be abundant. We treated infected dTHP1 cells with Jasp or Cyto D at 10 hpi for 4 h and examined for HA-M2 association using PLA at 14 hpi. Since Jasp and phalloidin compete for binding to the same site on F-actin (50), we were unable to use phalloidin staining to determine the effect of Jasp treatment on the actin cytoskeleton in dTHP1 cells. However, using an actin fractionation assay (51), we confirmed that treatment with Jasp for 4 h increases the ratio of insoluble (i.e., polymerized) actin to soluble actin in dTHP1 cells, in comparison to vehicle-treated cells (Fig. S5A). Under these conditions, most Jasp-treated dTHP1 cells showed reduced HA-M2 PLA signal, in comparison to vehicle- or Cyto D-treated cells (Fig. 8A and B). We note that surface HA and M2 expression in Jasp-treated cells was somewhat reduced relative to that in vehicle-treated cells (Fig. S5B and C). However, this reduction in surface expression of HA and M2 does not explain the decrease in HA-M2 PLA signal upon Jasp treatment; when HA or M2 expression on the cell surface and number of HA-M2 PLA spots were simultaneously assessed in the same cells, little correlation was observed between them (Fig. S6). Despite diminished HA-M2 association, vRNA release efficiency of Jasp-treated cells was not reduced in comparison to those of vehicle- and Cyto D-treated cells (Fig. 8C), suggesting that HA-M2 association, as measured by PLA, may not play as important a role in virus particle assembly/release in dTHP1 cells as it does in MDM (see Discussion). Consistent with this possibility, at 14 hpi, no obvious difference was observed in virus bud formation on the cell surface of dTHP1 cells following 4 h of treatment with Jasp versus vehicle or Cyto D (Fig. S7).

It is important to emphasize, however, that the defect in HA-M2 association is rescued upon inhibition of actin polymerization in MDM, while it is induced upon stabilization of actin in dTHP1 cells. Therefore, regardless of the effect on release of assembled particles, our data overall highlight a macrophage-specific role for actin polymerization in suppressing association between HA and M2 at the plasma membrane.

DISCUSSION

In a previous study, a posttranslational defect in productive IAV infection was observed in human MDM (33). A similar defect was also reported for murine macrophages in one study (29) but not the other (33). The exact nature of these defects that lead to inefficient IAV production has not been determined. Here, we have shown that despite efficient trafficking of the viral glycoproteins to the cell surface (Fig. 3), infectious virus particle formation at the plasma membrane is inefficient in human MDM (Fig. 2 and 4). The current study further identified HA-M2 association as an IAV assembly step suppressed in MDM (Fig. 5). This restriction is specific to primary macrophages, as the THP1 monocytic cell line differentiated to macrophage-like cells (dTHP1 cells) supports HA-M2 association and efficient IAV production. Notably, defective HA-M2 association and bud formation in MDM can be ameliorated by the disruption of actin polymerization, revealing a role for the actin cytoskeleton in suppressing IAV particle assembly in MDM (Fig. 6 and 7). However, virus particle release remains inefficient even when HA-M2 association and bud formation are restored by actin disruption (Fig. 7C), implying the presence of an additional defect in a postassembly step in MDM. Consistent with the restrictive role of actin polymerization, HA-M2 association in dTHP1 cells was blocked upon a treatment that promotes actin polymerization (Fig. 8).

Previous studies observed strain-specific differences for IAV replication in human macrophages. Some strains such as highly pathogenic H5N1 and pandemic 1918 strains can replicate in macrophages albeit at a lower efficiency than in epithelial cells (27, 28, 31, 34). Marvin et al. recently reported that the laboratory strain WSN is able to overcome blocks in IAV replication in human macrophages, while replication of the A/California/04/2009 strain is completely blocked (33). In our study, we observed that all tested strains, including WSN and A/California/04/2009, released significantly lower titers in MDM than in dTHP1 cells (Fig. 1C). Thus, it is likely that the cell-type-specific difference observed in this study is distinct from the previously reported strain-specific difference.

In addition to identifying a defective step for IAV replication in primary human macrophages, our study also lends mechanistic insights into the assembly and budding process of IAV in host cells. IAV is thought to assemble in cholesterol-enriched microdomains, or membrane rafts, of the plasma membrane in host cells (52–55). HA and NA accumulate at these assembly sites (38–40, 44, 56), also known as the budozones, while the third transmembrane protein, M2, is suggested to localize at the edge of the budozone (41, 46, 57). Coclustering between HA and M2 has been observed at steady state in epithelial cells (45, 57, 58). However, the sequence of events leading to recruitment of M2 to the budozone is unknown. Whether there is a mechanism regulating these events, other than simple diffusion over the plasma membrane, also remains to be determined. Our PLA data suggest that different molecular mechanisms mediate association between HA and NA and association between HA and M2 at the plasma membrane. Consistent with this possibility, a recent study showed that NA but not M2 accelerates HA trafficking to the apical surface of epithelial cells, presumably through cotrafficking (56). Thus, recruitment of M2 to assembly sites enriched in HA (and perhaps NA) is a discrete and host-cell-dependent step in the IAV assembly process.

The actin cytoskeleton has been implicated in assembly of IAV particles, in particular formation of filamentous particles (6, 59, 60). However, the actin-dependent mechanism(s) regulating IAV assembly is not well understood. Previous studies have shown that disruption of actin dynamics by both inhibition of actin polymerization (6, 59) (by latrunculin A or cytochalasin D) and promotion of actin polymerization (59) (by jasplakinolide) disrupts filamentous IAV assembly. In contrast, our study showed that drugs inhibiting actin polymerization and depolymerization have distinct and opposing effects on HA-M2 association: blocking actin polymerization in IAV nonpermissive cells (MDM) restores HA-M2 association, whereas enhancement of polymerization in permissive cells (dTHP1 cells) reduces HA-M2 association. Therefore, it is likely that distinct

actin-dependent mechanisms regulate the association between HA and M2 at the plasma membrane and formation of filamentous particles. As for the mechanism regulating HA-M2 association, one can speculate that subcortical actin promotes the segregation of HA- and M2-enriched plasma membrane microdomains. Consistent with this possibility, previous studies support a role for actin polymerization in maintaining HA-enriched microdomains as compact and dense (61, 62).

Of note, even though particle assembly is enhanced in MDM upon disruption of the actin cytoskeleton, virus release still remains defective in this cell type (Fig. 7). This suggests that an additional defect(s), for example, incomplete scission between viral envelope and plasma membrane or tethering of nascent particles to the cell surface, occurs in MDM. In addition to the nature of this late defect, whether the defect manifests due to the absence of a host factor enabling virus release or whether it is caused by the presence of a restriction factor blocking release of assembled virus particles warrants further investigation. It is also possible that cytochalasin D treatment blocks the release of assembled virus particles in an MDM-specific manner. These results, together with the pleiotropic effects of actin perturbation discussed above, also highlight the importance of specifically examining individual steps (e.g., HA-M2 association) rather than just monitoring the final outcomes, i.e., virus release efficiencies or released virus titers, when assessing the effect(s) of actin disruption on the virus assembly/release process.

The cytoplasmic domain of M2 contains an amphipathic helix that plays a role in scission of the IAV particle after budding (41, 57, 63). In epithelial (MDCK) or epithelial-like (293T) cell lines, viruses or VLP systems lacking M2 or expressing mutant M2 proteins are still able to initiate particle assembly and budding, presumably driven by HA and NA (38, 64). However, these buds adopt an abnormal morphology and/or fail to undergo scission or release (41, 57, 63), the latter of which results in accumulation of particles at the cell surface. In contrast, MDM showed very few buds on their surface under conditions where HA-M2 association was impaired (Fig. 4 and 7). These results suggest that in MDM, M2 plays an earlier role(s) in the assembly of virus particles, which is not apparent with 293T or MDCK cells that express M2-deficient virus or VLP systems. Such an earlier role may require other functions of M2. For example, in addition to scission of nascent particles, M2 functions in recruitment of M1 and vRNP to assembly sites (45, 63, 65–69), which is important for initiation of IAV particle assembly or elongation of filamentous particles (63, 68, 70–76). A defect in incorporation of M1 and/or vRNP into budding virus particles due to the failure of M2 recruitment may also explain the reduction in infectivity per particle observed for MDM-derived virus relative to dTHP1-derived virus (Fig. 2B). We also do not rule out the possibility that a failure in association of M1 and/or vRNP with the assembly sites may contribute to the observed defect in M2-HA association specific to MDM.

While jasplakinolide reduces HA-M2 association in dTHP1 cells, no reduction in virus bud formation is observed under this condition (see Fig. S7 in the supplemental material), which is consistent with previous studies performed with M2-lacking viruses in epithelial cell lines (41, 57, 63). However, we do not observe an arrest in virus release from dTHP1 cells, which was observed in the previous studies using M2-deficient viruses. In this regard, it is important to note that, unlike cells infected with M2-lacking mutant viruses, dTHP1 cells treated with jasplakinolide still show a residual level of M2 recruitment based on HA-M2 association detected by PLA. It is possible that this residual level of HA-M2 association is sufficient to promote the scission of virus buds in dTHP1 cells.

Overall, in this study, we have compared IAV replication in MDM with that in dTHP1 cells and found that MDM replicate vRNA, express viral proteins, and traffic HA, NA, and M2 to the plasma membrane at levels similar to those in dTHP1 cells. However, MDM are defective in assembling virus particles, likely due to actin-dependent suppression of association between the viral transmembrane proteins HA and M2. Comparison of actin regulatory mechanisms operating in MDM and dTHP1 cells, which are of the same lineage, will likely facilitate identification of additional host cellular factors involved in the assembly stage of the IAV life cycle.

MATERIALS AND METHODS

Cells and reagents. Monocytes were isolated by plate adhesion from peripheral blood mononuclear cells, which were obtained from buffy coats derived from unidentified healthy donors (New York Blood Center, NY). Cells were cultured in RPMI 1640 (Gibco) supplemented with 10% fetal bovine serum (FBS, HyClone) for 7 days before they were used for experiments. THP1 (ATCC TIB202) cells were cultured in RPMI 1640 supplemented with 10% FBS, 1 mM sodium pyruvate (Gibco), and 0.05 mM 2-mercaptoethanol. To generate differentiated THP1 cells (dTHP1), THP1 cells were cultured in the medium containing 0.1 μ M phorbol 12-myristate 13-acetate (PMA; Sigma) and 0.1 μ M vitamin D3 (Sigma) for 2 to 3 days. Madin-Darby canine kidney (MDCK) cells were provided by Arnold S. Monto (University of Michigan) and were cultured in DMEM (Gibco) supplemented with 10% FBS and 25 mM HEPES. Human lung carcinoma cell line A549 was provided by Mike Bachman (University of Michigan) and was cultured in DMEM (Gibco) supplemented with 10% FBS and 25 mM HEPES. The human embryonic kidney-derived 293T cell line (ATCC) was cultured and maintained in DMEM (Lonza) supplemented with 10% FBS.

The following antibodies were used for immunofluorescence microscopy: mouse anti-HA monoclonal antibody (clone C179 [36]; TaKaRa), mouse anti-M2 monoclonal antibody (clone 14C2 [77]; ThermoFisher), mouse anti-vRNP monoclonal antibody (clone 61A5 [35]; a kind gift from Fumitaka Momose, Kitasato University), goat anti-HA antiserum (BEI NR-3148), mouse anti-transferrin receptor (TfR) monoclonal antibody (clone M-A712; BD Biosciences). Rabbit anti-NA antiserum was a kind gift from Christopher Brooke (University of Illinois). Mouse anti-actin (ACTN05) was purchased from ThermoFisher. All secondary antibodies used for immunofluorescence and Alexa Fluor 488-labeled phalloidin were purchased from ThermoFisher. Cytochalasin D and jasplakinolide were purchased from Sigma and reconstituted in DMSO and 100% ethanol, respectively.

Plasmids and virus stocks. A/WSN/1933 (H1N1) virus was generated by reverse genetics (78) using the 8 pPoll plasmids carrying different segments of IAV genome and the 4 pCAGGS plasmids that express the PA, PB1, PB2, and NP proteins. The titers of the stocks were determined using the plaque assay with MDCK cells. A/Wyoming/03/2003 (H3N2) [Wyoming (H3N2)], A/Panama/2007/1999 (H3N2) [Panama (H3N2)], and A/California/04/2009 (H1N1) [California (H1N1)] viruses were kind gifts from Arnold S. Monto (University of Michigan) and were received as low-passage-number stocks (less than 5 passages in MDCK cells) of virus isolated from clinical specimens. Virus infection was performed and monitored using the plaque assay and flow cytometry as described in Text S1 in the supplemental material.

Measurement of vRNA levels. Virus-containing cell culture supernatants were centrifuged at 3,000 rpm for 5 min in a microcentrifuge, filtered through a 0.45- μ m filter, and subjected to ultracentrifugation at 30,800 rpm (AH650 swinging bucket rotor, ThermoFisher) for 90 min to prepare virus pellets. Virus and cell-associated vRNA was measured using a previously described protocol (79). Briefly, total RNA was extracted from virus pellets and cell lysates using TRIzol reagent (Ambion) according to the manufacturer's protocol. cDNA was generated using random hexamer priming and the SuperScript III First-Strand Synthesis System (Invitrogen). Quantitative PCR was performed on a CFX96 Real Time PCR system (Bio-Rad) using Platinum SYBR Green pPCR SuperMix-UDG (ThermoFisher Scientific). Serial 10-fold dilutions of pPoll plasmids containing specific viral genes of WSN were used to generate a standard curve for quantification of cDNA copy number based on cycle threshold (C_T) values. The primer sequences are shown in Text S1 in the supplemental material.

Correlative fluorescence and scanning electron microscopy (CFSEM). CFSEM experiments were performed as described before (80). Briefly, cells cultured on gridded coverslips (Bellco Biotechnology) were infected with WSN at MOI 0.1. Cells were fixed with 4% PFA in PBS at 20 hpi. After rinsing in PBS, quenching of PFA with PBS containing 0.1 M glycine (Sigma), and blocking with PBS containing 3% bovine serum albumin (BSA, Sigma), cells were immunostained with mouse anti-HA and fluorescently labeled secondary antibody. Cells were imaged using a Leica Inverted SP5X confocal microscope with a 40 \times PL APO objective and 10 to 20 \times scanning zoom. After fluorescence imaging, cells were fixed with PBS containing 2.5% glutaraldehyde (Electron Microscopy Sciences), stained with 1% OsO₄, dehydrated in a series of ethanol washes, rinsed in hexamethyldisilazane (Electron Microscopy Sciences), and allowed to dry overnight. Coverslips were affixed to specimen mounts and sputter coated with gold for 90 s (Polaron). Cells were identified by their location on the gridded coverslip and imaged on an Amray 1910FEG scanning electron microscope at 5 to 10 kV. Fluorescence and SEM images were roughly brought into registration by scaling and rotating images in Adobe Illustrator, similarly to other correlative fluorescence/SEM studies (80). Landmarks used for registration included cell edges. Cell surface structures visible in SEM were manually classified as virus-like buds if they appeared spherical and near 100 nm in diameter. To identify HA clusters in fluorescence images unambiguously, we removed uniform nonpunctate HA signal from the images. To do this, we calculated a 20-pixel radius median filter and subtracted the median filtered image from the original using the *Image Calculator* function in ImageJ. The number of HA-positive puncta was measured in the background-subtracted fluorescence images using the *Analyze particle* function in ImageJ. Since MDM have substantial membrane folds on the cell surface, especially toward the center of the cell, we focused on areas toward the edge of the cells, which have a flatter topology, for quantification of efficiency of virus bud formation.

In situ proximity ligation assay (PLA). PLA was performed using the Duolink PLA fluorescence kit following the manufacturer's instruction (Sigma). Cells fixed with 4% PFA (nonpermeabilized) were incubated with the following primary antibody combinations: goat anti-HA and mouse anti-M2 for PLA and rabbit anti-NA for identification of infected cells, mouse anti-HA and rabbit anti-NA for PLA and goat anti-HA for identification of infected cells, or goat anti-HA and mouse anti-TfR for PLA and rabbit anti-NA for identification of infected cells. Detection of PLA signals and identification of infected cells were performed using PLA probes specific to goat, mouse, or rabbit IgG and Alexa Fluor-488-labeled secondary antibody recognizing anti-NA or

anti-HA, respectively. Cells were observed using a Leica Inverted SP5X Confocal Microscope System with a 63× objective. Z-stacks extending from the focal plane corresponding to the middle plane of the nucleus (identified by DAPI staining) to the bottom of cells were acquired for each cell, and the maximum intensity projection for each cell was constructed using ImageJ. The PLA signal in projection images was thresholded to eliminate weak and hazy background signal in the nucleus, and the number of PLA-positive spots was counted using the *Analyze particle* function in ImageJ.

Actin fractionation assay. Actin fractionation was performed as previously described (51). Briefly, dTHP1 cells were treated with 0.5% ethanol (vehicle) or 1 μM jasplakinolide for 4 h. Cells were incubated with cytoskeleton stabilization buffer (4 M glycerol, 25 mM PIPES, pH 6.9, 1 mM EGTA, 1 mM CaCl₂) containing 0.1% Triton X-100 for 2 to 3 min. Cells were centrifuged for 5 min at 7,500 × *g* at 4°C. The pellet was resuspended in the cytoskeleton stabilization buffer. Supernatant (S) and pellet (P) fractions were run on a reducing and denaturing polyacrylamide gel and analyzed by immunoblotting.

Statistical analysis. Statistical analyses were performed using GraphPad Prism version 7. Two-tailed paired Student's *t* test was used to calculate *P* values in Fig. 1 to 3 and Fig. S1 to S4. Two-tailed unpaired Student's *t* test was performed in Fig. 4 to 7.

SUPPLEMENTAL MATERIAL

Supplemental material for this article may be found at <https://doi.org/10.1128/mBio.01916-18>.

TEXT S1, DOCX file, 0.1 MB.

FIG S1, EPS file, 0.9 MB.

FIG S2, EPS file, 2.2 MB.

FIG S3, EPS file, 1 MB.

FIG S4, EPS file, 3.2 MB.

FIG S5, EPS file, 6.2 MB.

FIG S6, EPS file, 4.5 MB.

FIG S7, EPS file, 39 MB.

ACKNOWLEDGMENTS

We thank the members of our laboratories for helpful discussions and critical review of the manuscript. We thank Christopher Sumner for help with optimization of the *in situ* Proximity Ligation Assay. We would also like to thank M. Bachman, C. Brooke, F. Momose, and A. S. Monto for reagents and Adam Lauring and his laboratory for advice on experimental protocols used in this study. The following reagent was obtained through BEI Resources, NIAID, NIH: polyclonal anti-influenza virus H1 (H0) hemagglutinin (HA), A/Puerto Rico/8/1934 (H1N1), (antiserum, goat), NR-3148. The microscopy data presented in this study was collected at the BRCF Microscopy core, University of Michigan.

This work was supported by funding from the National Institutes of Health (R01 AI071727) (to A.O.), the Takeda Science Foundation (to T.N.), and Leading Advanced Projects for medical innovation (LEAP) from the Japan Agency for Medical Research and Development (AMED) (JP17am0001007) (to Y.K.). S.B. was supported by a Clayton Willison- and Emma Elizabeth Willison-Endowed Graduate Fellowship.

REFERENCES

- Rodgers BC, Mims CA. 1982. Influenza virus replication in human alveolar macrophages. *J Med Virol* 9:177–184. <https://doi.org/10.1002/jmv.1890090304>.
- Hartmann BM, Li W, Jia J, Patil S, Marjanovic N, Martínez-Romero C, Albrecht RA, Hayot F, García-Sastre A, Wetmur JG, Moran TM, Sealson SC. 2013. Mouse dendritic cell (DC) influenza virus infectivity is much lower than that for human DCs and is hemagglutinin subtype dependent. *J Virol* 87:1916–1918. <https://doi.org/10.1128/JVI.02980-12>.
- Graham AC, Hilmer KM, Zickovich JM, Obar JJ. 2013. Inflammatory response of mast cells during influenza A virus infection is mediated by active infection and RIG-I signaling. *J Immunol* 190:4676–4684. <https://doi.org/10.4049/jimmunol.1202096>.
- Lohmeyer J, Talens LT, Klenk HD. 1979. Biosynthesis of the influenza virus envelope in abortive infection. *J Gen Virol* 42:73–88. <https://doi.org/10.1099/0022-1317-42-1-73>.
- Gujuluva CN, Kundu A, Murti KG, Nayak DP. 1994. Abortive replication of influenza virus A/WSN/33 in HeLa229 cells: defective viral entry and budding processes. *Virology* 204:491–505. <https://doi.org/10.1006/viro.1994.1563>.
- Roberts PC, Compans RW. 1998. Host cell dependence of viral morphology. *Proc Natl Acad Sci U S A* 95:5746–5751. <https://doi.org/10.1073/pnas.95.10.5746>.
- Moncorgé O, Mura M, Barclay WS. 2010. Evidence for avian and human host cell factors that affect the activity of influenza virus polymerase. *J Virol* 84:9978–9986. <https://doi.org/10.1128/JVI.01134-10>.
- Mehle A, Doudna JA. 2008. An inhibitory activity in human cells restricts the function of an avian-like influenza virus polymerase. *Cell Host Microbe* 4:111–122. <https://doi.org/10.1016/j.chom.2008.06.007>.
- Feng Y, Broder CC, Kennedy PE, Berger EA. 1996. HIV-1 entry cofactor: functional cDNA cloning of a seven-transmembrane, G protein-coupled receptor. *Science* 272:872–877. <https://doi.org/10.1126/science.272.5263.872>.
- Bortz E, Westera L, Maamary J, Steel J, Albrecht RA, Manicassamy B, Chase G, Martínez-Sobrido L, Schwemmle M, García-Sastre A. 2011. Host-

- and strain-specific regulation of influenza virus polymerase activity by interacting cellular proteins. *mBio* 2:e00151-11. <https://doi.org/10.1128/mBio.00151-11>.
11. Hudjetz B, Gabriel G. 2012. Human-like PB2 627K influenza virus polymerase activity is regulated by importin- α 1 and - α 7. *PLoS Pathog* 8:e1002488. <https://doi.org/10.1371/journal.ppat.1002488>.
 12. Long JS, Giotis ES, Moncorgé O, Frise R, Mistry B, James J, Morisson M, Iqbal M, Vignal A, Skinner MA, Barclay WS. 2016. Species difference in ANP32A underlies influenza A virus polymerase host restriction. *Nature* 529:101–104. <https://doi.org/10.1038/nature16474>.
 13. Kuo SM, Chen CJ, Chang SC, Liu TJ, Chen YH, Huang SY, Shih SR. 2017. Inhibition of avian influenza A virus replication in human cells by host restriction factor TUFM is correlated with autophagy. *mBio* 8:e00481-17. <https://doi.org/10.1128/mBio.00481-17>.
 14. Laguette N, Sobhian B, Casarelli N, Ringard M, Chable-Bessia C, Ségéral E, Yatim A, Emiliani S, Schwartz O, Benkirane M. 2011. SAMHD1 is the dendritic- and myeloid-cell-specific HIV-1 restriction factor counteracted by Vpx. *Nature* 474:654–657. <https://doi.org/10.1038/nature10117>.
 15. Neil SJ, Zang T, Bieniasz PD. 2008. Tetherin inhibits retrovirus release and is antagonized by HIV-1 Vpu. *Nature* 451:425–430. <https://doi.org/10.1038/nature06553>.
 16. Sheehy AM, Gaddis NC, Choi JD, Malim MH. 2002. Isolation of a human gene that inhibits HIV-1 infection and is suppressed by the viral Vif protein. *Nature* 418:646–650. <https://doi.org/10.1038/nature00939>.
 17. Hao L, Sakurai A, Watanabe T, Sorensen E, Nidom CA, Newton MA, Ahlquist P, Kawaoka Y. 2008. Drosophila RNAi screen identifies host genes important for influenza virus replication. *Nature* 454:890–893. <https://doi.org/10.1038/nature07151>.
 18. Shapira SD, Gat-Viks I, Shum BO, Dricot A, de Grace MM, Wu L, Gupta PB, Hao T, Silver SJ, Root DE, Hill DE, Regev A, Hacohen N. 2009. A physical and regulatory map of host-influenza interactions reveals pathways in H1N1 infection. *Cell* 139:1255–1267. <https://doi.org/10.1016/j.cell.2009.12.018>.
 19. Karlas A, Machuy N, Shin Y, Pleissner KP, Artarini A, Heuer D, Becker D, Khalil H, Ogilvie LA, Hess S, Mäurer AP, Müller E, Wolff T, Rudel T, Meyer TF. 2010. Genome-wide RNAi screen identifies human host factors crucial for influenza virus replication. *Nature* 463:818–822. <https://doi.org/10.1038/nature08760>.
 20. König R, Stertz S, Zhou Y, Inoue A, Hoffmann HH, Bhattacharyya S, Alamares JG, Tscherner DM, Ortigoza MB, Liang Y, Gao Q, Andrews SE, Bandyopadhyay S, De Jesus P, Tu BP, Pache L, Shih C, Orth A, Bonamy G, Miraglia L, Ideker T, García-Sastre A, Young JA, Palese P, Shaw ML, Chanda SK. 2010. Human host factors required for influenza virus replication. *Nature* 463:813–817. <https://doi.org/10.1038/nature08699>.
 21. Su WC, Chen YC, Tseng H, Hsu PW, Tung KF, Jeng KS, Lai MM. 2013. Pooled RNAi screen identifies ubiquitin ligase Itch as crucial for influenza A virus release from the endosome during virus entry. *Proc Natl Acad Sci U S A* 110:17516–17521. <https://doi.org/10.1073/pnas.1312374110>.
 22. Watanabe T, Kawakami E, Shoemaker JE, Lopes TJ, Matsuoka Y, Tomita Y, Kozuka-Hata H, Gorai T, Kuwahara T, Takeda E, Nagata A, Takano R, Kiso M, Yamashita M, Sakai-Tagawa Y, Katsura H, Nonaka N, Fujii H, Fujii K, Sugita Y, Noda T, Goto H, Fukuyama S, Watanabe S, Neumann G, Oyama M, Kitano H, Kawaoka Y. 2014. Influenza virus-host interactome screen as a platform for antiviral drug development. *Cell Host Microbe* 16:795–805. <https://doi.org/10.1016/j.chom.2014.11.002>.
 23. Tripathi S, Pohl MO, Zhou Y, Rodriguez-Frandsen A, Wang G, Stein DA, Moulton HM, DeJesus P, Che J, Mulder LC, Yáñez E, Andenmatten D, Pache L, Manicassamy B, Albrecht RA, Gonzalez MG, Nguyen Q, Brass A, Elledge S, White M, Shapira S, Hacohen N, Karlas A, Meyer TF, Shales M, Gatorano A, Johnson JR, Jang G, Johnson T, Verschuere E, Sanders D, Krogan N, Shaw M, König R, Stertz S, García-Sastre A, Chanda SK. 2015. Meta- and orthogonal integration of influenza “OMICs” data defines a role for UBR4 in virus budding. *Cell Host Microbe* 18:723–735. <https://doi.org/10.1016/j.chom.2015.11.002>.
 24. Meliopoulos VA, Andersen LE, Birrer KF, Simpson KJ, Lowenthal JW, Bean AG, Stambas J, Stewart CR, Tompkins SM, van Beusechem VW, Fraser I, Mhlanga M, Barichievy S, Smith Q, Leake D, Karpilow J, Buck A, Jona G, Tripp RA. 2012. Host gene targets for novel influenza therapies elucidated by high-throughput RNA interference screens. *FASEB J* 26:1372–1386. <https://doi.org/10.1096/fj.11-193466>.
 25. Heaton NS, Moshkina N, Fenouil R, Gardner TJ, Aguirre S, Shah PS, Zhao N, Manganaro L, Hultquist JF, Noel J, Sachs D, Hamilton J, Leon PE, Chawdury A, Tripathi S, Melegari C, Campisi L, Hai R, Metreveli G, Gamarnik AV, García-Sastre A, Greenbaum B, Simon V, Fernandez-Sesma A, Krogan NJ, Mulder LCF, van Bakel H, Tortorella D, Taunton J, Palese P, Marazzi I. 2016. Targeting viral proteostasis limits influenza virus, HIV, and dengue virus infection. *Immunity* 44:46–58. <https://doi.org/10.1016/j.immuni.2015.12.017>.
 26. Heaton BE, Kennedy EM, Dumm RE, Harding AT, Sacco MT, Sachs D, Heaton NS. 2017. A CRISPR activation screen identifies a pan-avian influenza virus inhibitory host factor. *Cell Rep* 20:1503–1512. <https://doi.org/10.1016/j.celrep.2017.07.060>.
 27. Cline TD, Karlsson EA, Seufzer BJ, Schultz-Cherry S. 2013. The hemagglutinin protein of highly pathogenic H5N1 influenza viruses overcomes an early block in the replication cycle to promote productive replication in macrophages. *J Virol* 87:1411–1419. <https://doi.org/10.1128/JVI.02682-12>.
 28. Yu WC, Chan RW, Wang J, Travanty EA, Nicholls JM, Peiris JS, Mason RJ, Chan MC. 2011. Viral replication and innate host responses in primary human alveolar epithelial cells and alveolar macrophages infected with influenza H5N1 and H1N1 viruses. *J Virol* 85:6844–6855. <https://doi.org/10.1128/JVI.02200-10>.
 29. Londrigan SL, Short KR, Ma J, Gillespie L, Rockman SP, Brooks AG, Reading PC. 2015. Infection of mouse macrophages by seasonal influenza viruses can be restricted at the level of virus entry and at a late stage in the virus life cycle. *J Virol* 89:12319–12329. <https://doi.org/10.1128/JVI.01455-15>.
 30. Mok CK, Lee DC, Cheung CY, Peiris M, Lau AS. 2007. Differential onset of apoptosis in influenza A virus H5N1- and H1N1-infected human blood macrophages. *J Gen Virol* 88:1275–1280. <https://doi.org/10.1099/vir.0.82423-0>.
 31. Sakabe S, Iwatsuki-Horimoto K, Takano R, Nidom CA, Le M, Nagamura-Inoue T, Horimoto T, Yamashita N, Kawaoka Y. 2011. Cytokine production by primary human macrophages infected with highly pathogenic H5N1 or pandemic H1N1 2009 influenza viruses. *J Gen Virol* 92:1428–1434. <https://doi.org/10.1099/vir.0.030346-0>.
 32. van Riel D, Leijten LM, van der Eerden M, Hoogsteden HC, Boven LA, Lambrecht BN, Osterhaus AD, Kuiken T. 2011. Highly pathogenic avian influenza virus H5N1 infects alveolar macrophages without virus production or excessive TNF- α induction. *PLoS Pathog* 7:e1002099. <https://doi.org/10.1371/journal.ppat.1002099>.
 33. Marvin SA, Russier M, Huerta CT, Russell CJ, Schultz-Cherry S. 2017. Influenza overcomes cellular blocks to productively replicate, impacting macrophage function. *J Virol* 91:e01417-16. <https://doi.org/10.1128/JVI.01417-16>.
 34. Perrone LA, Plowden JK, García-Sastre A, Katz JM, Tumpey TM. 2008. H5N1 and 1918 pandemic influenza virus infection results in early and excessive infiltration of macrophages and neutrophils in the lungs of mice. *PLoS Pathog* 4:e1000115. <https://doi.org/10.1371/journal.ppat.1000115>.
 35. Momose F, Kikuchi Y, Komase K, Morikawa Y. 2007. Visualization of microtubule-mediated transport of influenza viral progeny ribonucleoprotein. *Microbes Infect* 9:1422–1433. <https://doi.org/10.1016/j.micinf.2007.07.007>.
 36. Okuno Y, Isegawa Y, Sasao F, Ueda S. 1993. A common neutralizing epitope conserved between the hemagglutinins of influenza A virus H1 and H2 strains. *J Virol* 67:2552–2558.
 37. Doud MB, Lee JM, Bloom JD. 2018. How single mutations affect viral escape from broad and narrow antibodies to H1 influenza hemagglutinin. *Nat Commun* 9:1386. <https://doi.org/10.1038/s41467-018-03665-3>.
 38. Chen BJ, Leser GP, Morita E, Lamb RA. 2007. Influenza virus hemagglutinin and neuraminidase, but not the matrix protein, are required for assembly and budding of plasmid-derived virus-like particles. *J Virol* 81:7111–7123. <https://doi.org/10.1128/JVI.00361-07>.
 39. Leser GP, Lamb RA. 2005. Influenza virus assembly and budding in raft-derived microdomains: a quantitative analysis of the surface distribution of HA, NA and M2 proteins. *Virology* 342:215–227. <https://doi.org/10.1016/j.virol.2005.09.049>.
 40. Takeda M, Leser GP, Russell CJ, Lamb RA. 2003. Influenza virus hemagglutinin concentrates in lipid raft microdomains for efficient viral fusion. *Proc Natl Acad Sci U S A* 100:14610–14617. <https://doi.org/10.1073/pnas.2235620100>.
 41. Rossman JS, Jing X, Leser GP, Lamb RA. 2010. Influenza virus M2 protein mediates ESCRT-independent membrane scission. *Cell* 142:902–913. <https://doi.org/10.1016/j.cell.2010.08.029>.
 42. Kawaguchi A, Hirohama M, Harada Y, Osari S, Nagata K. 2015. Influenza virus induces cholesterol-enriched endocytic recycling compartments for budzone formation via cell cycle-independent centrosome matu-

- ration. *PLoS Pathog* 11:e1005284. <https://doi.org/10.1371/journal.ppat.1005284>.
43. Harder T, Scheiffele P, Verkade P, Simons K. 1998. Lipid domain structure of the plasma membrane revealed by patching of membrane components. *J Cell Physiol* 141:929–942.
 44. Zhang J, Pekosz A, Lamb RA. 2000. Influenza virus assembly and lipid raft microdomains: a role for the cytoplasmic tails of the spike glycoproteins. *J Virol* 74:4634–4644. <https://doi.org/10.1128/JVI.74.10.4634-4644.2000>.
 45. Chen BJ, Leser GP, Jackson D, Lamb RA. 2008. The influenza virus M2 protein cytoplasmic tail interacts with the M1 protein and influences virus assembly at the site of virus budding. *J Virol* 82:10059–10070. <https://doi.org/10.1128/JVI.01184-08>.
 46. Rossman JS, Jing X, Leser GP, Balannik V, Pinto LH, Lamb RA. 2010. Influenza virus m2 ion channel protein is necessary for filamentous virion formation. *J Virol* 84:5078–5088. <https://doi.org/10.1128/JVI.00119-10>.
 47. Liu AP, Fletcher DA. 2006. Actin polymerization serves as a membrane domain switch in model lipid bilayers. *Biophys J* 91:4064–4070. <https://doi.org/10.1529/biophysj.106.090852>.
 48. Gaus K, Chklovskaya E, Fazekas de St Groth B, Jessup W, Harder T. 2005. Condensation of the plasma membrane at the site of T lymphocyte activation. *J Cell Physiol* 171:121–131. <https://doi.org/10.1083/jcb.200505047>.
 49. Chichili GR, Rodgers W. 2007. Clustering of membrane raft proteins by the actin cytoskeleton. *J Biol Chem* 282:36682–36691. <https://doi.org/10.1074/jbc.M702959200>.
 50. Bubb MR, Senderowicz AM, Sausville EA, Duncan KL, Korn ED. 1994. Jaspilkinolide, a cytotoxic natural product, induces actin polymerization and competitively inhibits the binding of phalloidin to F-actin. *J Biol Chem* 269:14869–14871.
 51. Freeman SA, Vega A, Riedl M, Collins RF, Ostrowski PP, Woods EC, Bertozzi CR, Tammi MI, Lidke DS, Johnson P, Mayor S, Jaqaman K, Grinstein S. 2018. Transmembrane pickets connect cyto- and pericellular skeletons forming barriers to receptor engagement. *Cell* 172:305–317.e10. <https://doi.org/10.1016/j.cell.2017.12.023>.
 52. Schmitt AP, Lamb RA. 2005. Influenza virus assembly and budding at the viral budzone. *Adv Virus Res* 64:383–416. [https://doi.org/10.1016/S0065-3527\(05\)64012-2](https://doi.org/10.1016/S0065-3527(05)64012-2).
 53. Veit M, Thaa B. 2011. Association of influenza virus proteins with membrane rafts. *Adv Virol* 2011:370606. <https://doi.org/10.1155/2011/370606>.
 54. Rossman JS, Lamb RA. 2011. Influenza virus assembly and budding. *Virology* 411:229–236. <https://doi.org/10.1016/j.virol.2010.12.003>.
 55. Nayak DP, Balogun RA, Yamada H, Zhou ZH, Barman S. 2009. Influenza virus morphogenesis and budding. *Virus Res* 143:147–161. <https://doi.org/10.1016/j.virusres.2009.05.010>.
 56. Ohkura T, Momose F, Ichikawa R, Takeuchi K, Morikawa Y. 2014. Influenza A virus hemagglutinin and neuraminidase mutually accelerate their apical targeting through clustering of lipid rafts. *J Virol* 88:10039–10055. <https://doi.org/10.1128/JVI.00586-14>.
 57. Roberts KL, Leser GP, Ma C, Lamb RA. 2013. The amphipathic helix of influenza A virus M2 protein is required for filamentous bud formation and scission of filamentous and spherical particles. *J Virol* 87:9973–9982. <https://doi.org/10.1128/JVI.01363-13>.
 58. Leser GP, Lamb RA. 2017. Lateral organization of influenza virus proteins in the budzone region of the plasma membrane. *J Virol* 91:e02104-16. <https://doi.org/10.1128/JVI.02104-16>.
 59. Simpson-Holley M, Ellis D, Fisher D, Elton D, McCauley J, Digard P. 2002. A functional link between the actin cytoskeleton and lipid rafts during budding of filamentous influenza virions. *Virology* 301:212–225. <https://doi.org/10.1006/viro.2002.1595>.
 60. Kumakura M, Kawaguchi A, Nagata K. 2015. Actin-myosin network is required for proper assembly of influenza virus particles. *Virology* 476:141–150. <https://doi.org/10.1016/j.virol.2014.12.016>.
 61. Gunewardene MS, Subach FV, Gould TJ, Penoncello GP, Gudheti MV, Verkhusha VV, Hess ST. 2011. Superresolution imaging of multiple fluorescent proteins with highly overlapping emission spectra in living cells. *Biophys J* 101:1522–1528. <https://doi.org/10.1016/j.bpj.2011.07.049>.
 62. Gudheti MV, Curthoys NM, Gould TJ, Kim D, Gunewardene MS, Gabor KA, Gosse JA, Kim CH, Zimmerberg J, Hess ST. 2013. Actin mediates the nanoscale membrane organization of the clustered membrane protein influenza hemagglutinin. *Biophys J* 104:2182–2192. <https://doi.org/10.1016/j.bpj.2013.03.054>.
 63. Iwatsuki-Horimoto K, Horimoto T, Noda T, Kiso M, Maeda J, Watanabe S, Muramoto Y, Fujii K, Kawaoka Y. 2006. The cytoplasmic tail of the influenza A virus M2 protein plays a role in viral assembly. *J Virol* 80:5233–5240. <https://doi.org/10.1128/JVI.00049-06>.
 64. Chlanda P, Schraidt O, Kummer S, Riches J, Oberwinkler H, Prinz S, Kräusslich HG, Briggs JA. 2015. Structural analysis of the roles of influenza A virus membrane-associated proteins in assembly and morphology. *J Virol* 89:8957–8966. <https://doi.org/10.1128/JVI.00592-15>.
 65. McCown MF, Pekosz A. 2006. Distinct domains of the influenza A virus M2 protein cytoplasmic tail mediate binding to the M1 protein and facilitate infectious virus production. *J Virol* 80:8178–8189. <https://doi.org/10.1128/JVI.00627-06>.
 66. McCown MF, Pekosz A. 2005. The influenza A virus M2 cytoplasmic tail is required for infectious virus production and efficient genome packaging. *J Virol* 79:3595–3605. <https://doi.org/10.1128/JVI.79.6.3595-3605.2005>.
 67. Su WC, Yu WY, Huang SH, Lai MMC. 2018. Ubiquitination of the cytoplasmic domain of influenza A virus M2 protein is crucial for production of infectious virus particles. *J Virol* 92:e01972-17. <https://doi.org/10.1128/JVI.01972-17>.
 68. Grantham ML, Stewart SM, Lalime EN, Pekosz A. 2010. Tyrosines in the influenza A virus M2 protein cytoplasmic tail are critical for production of infectious virus particles. *J Virol* 84:8765–8776. <https://doi.org/10.1128/JVI.00853-10>.
 69. Wang D, Harmon A, Jin J, Francis DH, Christopher-Hennings J, Nelson E, Montelaro RC, Li F. 2010. The lack of an inherent membrane targeting signal is responsible for the failure of the matrix (M1) protein of influenza A virus to bud into virus-like particles. *J Virol* 84:4673–4681. <https://doi.org/10.1128/JVI.02306-09>.
 70. Burleigh LM, Calder LJ, Skehel JJ, Steinhauer DA. 2005. Influenza A viruses with mutations in the m1 helix six domain display a wide variety of morphological phenotypes. *J Virol* 79:1262–1270. <https://doi.org/10.1128/JVI.79.2.1262-1270.2005>.
 71. Amorim MJ, Bruce EA, Read EK, Foeglein A, Mahen R, Stuart AD, Digard P. 2011. A Rab11- and microtubule-dependent mechanism for cytoplasmic transport of influenza A virus viral RNA. *J Virol* 85:4143–4156. <https://doi.org/10.1128/JVI.02606-10>.
 72. Bourmakina SV, García-Sastre A. 2005. The morphology and composition of influenza A virus particles are not affected by low levels of M1 and M2 proteins in infected cells. *J Virol* 79:7926–7932. <https://doi.org/10.1128/JVI.79.12.7926-7932.2005>.
 73. Moreira É, Weber A, Bolte H, Kolesnikova L, Giese S, Lakdawala S, Beer M, Zimmer G, García-Sastre A, Schwemmler M, Juozapaitis M. 2016. A conserved influenza A virus nucleoprotein code controls specific viral genome packaging. *Nat Commun* 7:12861. <https://doi.org/10.1038/ncomms12861>.
 74. Elleman CJ, Barclay WS. 2004. The M1 matrix protein controls the filamentous phenotype of influenza A virus. *Virology* 321:144–153. <https://doi.org/10.1016/j.virol.2003.12.009>.
 75. Roberts PC, Lamb RA, Compans RW. 1998. The M1 and M2 proteins of influenza A virus are important determinants in filamentous particle formation. *Virology* 240:127–137. <https://doi.org/10.1006/viro.1997.8916>.
 76. Liu H, Grantham ML, Pekosz A. 2018. Mutations in the influenza A virus M1 protein enhance virus budding to complement lethal mutations in the M2 cytoplasmic tail. *J Virol* 92:e00858-17. <https://doi.org/10.1128/JVI.00858-17>.
 77. Zebedee SL, Lamb RA. 1988. Influenza A virus M2 protein: monoclonal antibody restriction of virus growth and detection of M2 in virions. *J Virol* 62:2762–2772.
 78. Neumann G, Watanabe T, Ito H, Watanabe S, Goto H, Gao P, Hughes M, Perez DR, Donis R, Hoffmann E, Hobom G, Kawaoka Y. 1999. Generation of influenza A viruses entirely from cloned cDNAs. *Proc Natl Acad Sci U S A* 96:9345–9350. <https://doi.org/10.1073/pnas.96.16.9345>.
 79. Pauly MD, Lauring AS. 2015. Effective lethal mutagenesis of influenza virus by three nucleoside analogs. *J Virol* 89:3584–3597. <https://doi.org/10.1128/JVI.03483-14>.
 80. Hogue IB, Grover JR, Soheilian F, Nagashima K, Ono A. 2011. Gag induces the coalescence of clustered lipid rafts and tetraspanin-enriched microdomains at HIV-1 assembly sites on the plasma membrane. *J Virol* 85:9749–9766. <https://doi.org/10.1128/JVI.00743-11>.